

ULSAM: Ultra-Lightweight Subspace Attention Module for Compact Convolutional Neural Networks

Rajat Saini*
IIT Hyderabad

cs17mtech11002@iith.ac.in

Nandan Kumar Jha*†
IIT Hyderabad

cs17mtech11010@iith.ac.in

Bedanta Das
IIT Hyderabad

cs17mtech11009@iith.ac.in

Sparsh Mittal
IIT Roorkee

sparshfec@iitr.ac.in

C. Krishna Mohan
IIT Hyderabad

ckm@iith.ac.in

Abstract

The capability of the self-attention mechanism to model the long-range dependencies has catapulted its deployment in vision models. Unlike convolution operators, self-attention offers infinite receptive field and enables compute-efficient modeling of global dependencies. However, the existing state-of-the-art attention mechanisms incur high compute and/or parameter overheads, and hence unfit for compact convolutional neural networks (CNNs). In this work, we propose a simple yet effective “Ultra-Lightweight Subspace Attention Mechanism” (ULSAM), which infers different attention maps for each feature map subspace. We argue that learning separate attention maps for each feature subspace enables multi-scale and multi-frequency feature representation, which is more desirable for fine-grained image classification. Our method of subspace attention is orthogonal and complementary to the existing state-of-the-arts attention mechanisms used in vision models. ULSAM is end-to-end trainable and can be deployed as a plug-and-play module in the pre-existing compact CNNs. Notably, our work is the first attempt that uses a subspace attention mechanism to increase the efficiency of compact CNNs. To show the efficacy of ULSAM, we perform experiments with MobileNet-V1 and MobileNet-V2 as backbone architectures on ImageNet-1K and three fine-grained image classification datasets. We achieve $\approx 13\%$ and $\approx 25\%$ reduction in both the FLOPs and parameter counts of MobileNet-V2 with a 0.27% and more than 1% improvement in top-1 accuracy on the ImageNet-1K and fine-grained image classification datasets (respectively). Code and trained models are available at <https://github.com/Nandan91/ULSAM>.

*The first two authors contributed equally to this work.

†Corresponding author.

1. Introduction

Convolutional neural networks (CNNs) have achieved remarkable predictive performance in various cognitive and learning tasks [11, 43, 12, 32, 18]. The unprecedented predictive performance of CNNs stems from the rich representational power of CNNs, which in turn stems from the deeper and wider layers in networks. Deeper and wider layers enhance the expressiveness and discrimination ability of the network by circumventing the inherent limitations of convolution operators, viz., locality [7] and linearity [20].

The locality of the seminal operator, convolution, in CNNs offers a theoretical guarantee, unlike the shallow networks, to avoid the *curse of dimensionality* while approximating the hierarchically local compositional functions [27, 22]. Since convolution in CNN capture the local (e.g., 3×3) feature correlations [19], multiple convolution operators are stacked together to enlarge the effective receptive field size and capture the long-range dependencies [7]. However, this makes the CNNs *deeper*. Further, since the linearity of convolution operation leads to inefficient capturing of the non-linear abstractions in input data [20], CNNs employ a higher number of filters per layer, which are learned to capture all the possible variations of complex latent concept [20]. However, this makes the CNNs *wider*. Deeper and wider layers in CNNs [12, 43, 13] leads to a high computational cost (measured in the number of floating-point operations or FLOPs) and a large number of parameters which makes deployment of CNNs on resources-constrained platforms quite challenging.

The compact CNNs such as MobileNets [14, 30] and ShuffleNets [48, 21] seek to reduce the computational cost significantly by employing depthwise separable (DWS) convolution. Similarly, the dilated convolution has been employed to enlarge the receptive field size in vision tasks [45]. However, the inefficiencies of convolution operators

still exist, and the network learns complex cross channel inter-dependencies in a computationally-inefficient manner.

The success of self-attention in natural language processing [36] in modeling the long-range dependencies has enabled its inclusion as a computation primitive in vision models [28, 1, 7]. Self-attention efficiently captures the global dependencies of features in feature space and circumvents the inherent limitations of convolution operators in CNNs. However, the higher parameters and/or computation overheads of these attention mechanisms (Table 1) are undesirable for in compact CNNs. Since redundancy in the parameter space of compact CNNs is low, the desirable attention mechanism for compact CNNs should have the capability to capture the global correlation (fusing semantic and spatial information) more effectively and efficiently compared to the existing attention mechanism.

In this work, we propose the ‘‘Ultra-Lightweight subspace attention module’’ (ULSAM), a novel attention block for compact CNNs (Figure 1). ULSAM learns different attention maps for each feature map subspace and reduces the spatial and channel redundancy in feature maps of compact CNNs. Also, learning different attention maps for each subspace enables multi-scale and multi-frequency feature representation, which is desirable, especially for the fine-grained image classification tasks. To the best of our knowledge, ULSAM is the first attention module which enables efficient (compute and parameter) learning of cross channel inter-dependencies in each subspace of feature maps.

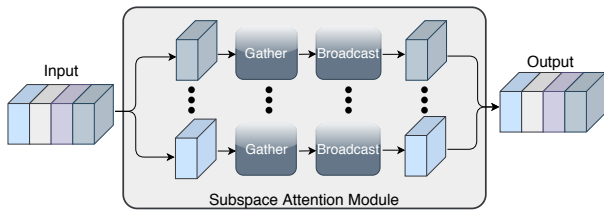


Figure 1. A block diagram of ULSAM

Our key contributions are summarized as follows:

- We propose a novel attention block (ULSAM) for compact CNNs, which learns individual attention maps for each feature subspace and enables compute-efficient learning of cross-channel information along with multi-scale and multi-frequency feature learning.
- We show the effectiveness of our block (ULSAM) through extensive experiments with MobileNet-V1 and MobileNet-V2 on ImageNet-1K as well as three fine-grained image classification datasets.
- We demonstrate the scalability and efficacy of ULSAM with fewer parameters and computations on MobileNet-V1 and MobileNet-V2 with ImageNet-1K and fine-grained datasets.

2. Background and Related Work

This section describes various design techniques, along with their limitations, which have been incorporated in CNNs to reduce the number of FLOPs. Further, we brief state-of-the-art attention mechanisms employed in vision models for reducing the FLOPs and parameter counts by virtue of feature re-distribution in the feature space. We show the overhead, in terms of FLOPs and parameters counts, of these attention mechanisms along with our proposed module, ULSAM, in Table 1.

2.1. Computational Cost of Convolution in CNNs

The computational cost (in FLOPs) of standard convolution (SConv) and FC layers of filter size $s_k \times s_k$ is shown in Eq. 1, where m and n are the number of input feature maps and output feature maps (respectively) of spatial size $h \times w$. Note that the FC layer is a special case of the convolution layer where the filter size is equal to the input feature map size, and hence, the size of output feature maps size in the FC layer is 1×1 .

$$\text{FLOPs in SConv} = s_k \times s_k \times m \times n \times h \times w \quad (1)$$

In state-of-the-art CNNs [30, 14, 12], m and n are in the order of thousands (in deeper layers of CNNs) hence, the value of $m \times n$ is substantially large. In Eq. 1, the term $m \times n$ coupled with $s_k \times s_k$ stems from the combined feature extraction and feature aggregation in SConv. To reduce the computational cost depthwise separable (DWS) convolution [30, 14, 9] has been deployed which decouples the $m \times n$ with $s_k \times s_k$ by decomposing the standard convolution into depthwise convolution (feature extraction) and pointwise convolution (feature aggregation). Depthwise convolution reduces redundancy in the channel extent and breaks the fully connected pattern between input and output feature. Similarly, pointwise convolution reduces the redundancy in the spatial extent. The computational cost of DWS convolution is $s_k \times s_k \times m \times h \times w$ (depthwise conv) + $m \times n \times h \times w$ (pointwise conv). This decomposition in DWS convolution reduces the computations significantly; however, due to the $m \times n$ term in pointwise convolution, the computations in DWS convolution are dominated by the pointwise convolution. For example, in MobileNet-V1 [14], pointwise convolution accounts for 94.86% of the total FLOPs while depthwise convolution accounts for only 3.06% of the total FLOPs.

To reduce the computation overhead of pointwise convolution, ShuffleNet [48] employs group convolution on 1×1 layers. In group convolution, input feature maps are divided into mutually exclusive groups, and each group independently convolves with $s_k \times s_k$ filters and breaks the fully-connected patterns among input and output features

Table 1. Compute and parameter overheads of different attention modules. These overheads are compared with our proposed attention module ‘‘ULSAM’’ (assuming $m = 512$, $t = \frac{m}{8}$, $r = 16$, $h \times w = 14 \times 14$, and dilation rate is 4 in BAM [25]).

Attention module	subspace attention	MLP	costlier 1×1 conv	#Params	#FLOPs	#Params ($\times 10^3$)	#FLOPs ($\times 10^6$)	#Params (<i>norm.</i>)	#FLOPs (<i>norm.</i>)
Non-local [39]	×	×	✓	$2m^2$	$2m^2hw$	524	102.76	$512\times$	$512\times$
A^2 - Net [7]	×	×	✓	$2mt$	$2mthw$	66	12.85	$64\times$	$64\times$
SE-Net [15]	×	✓	×	$\frac{2m^2}{r}$	$\frac{2m^2}{r}$	33	0.03	$33\times$	$0.16\times$
BAM [25]	×	✓	✓	$\frac{4m^2}{r} + \frac{18m^2}{r^2}$	$\frac{2m^2}{r} + (\frac{4m^2}{r} + \frac{18m^2}{r^2})hw$	84	16.49	$82\times$	$82.16\times$
CBAM [42]	×	✓	×	$\frac{2m^2}{r} + 98$	$\frac{2m^2}{r} + 98hw$	33	0.05	$33\times$	$0.26\times$
ULSAM (ours)	✓	×	×	$2m$	$2mhw$	1	0.2	$1\times$	$1\times$

maps. This reduces the number of computations; however, the stacking of multiple group convolution layers prohibits the cross-group interaction and leads to a drop in performance [48]. To tackle this issue, ShuffleNet employs the channel shuffling mechanism after the group convolution layer. However, the channel shuffling does not scale with a larger number of groups, and with an increasing number of groups, channel shuffling gives diminishing returns [48]. Also, channel shuffling is naive and context-unaware, and hence, the limitations of group convolution are not adequately mitigated.

ULSAM employs attention mechanism and enables compute-efficient interaction of cross-channel information where only one 1×1 filter is used after depthwise convolution, i.e., $n=1$ and there is no $m \times n$ term in the computation. Therefore, ULSAM decomposes the dense connections among input and output feature maps *without incurring the limitations of group convolution and computation overhead of pointwise convolution*.

2.2. Attention Mechanisms for Vision Models

In guided cognition tasks, attention is a way to assign different importance to different parts of the input data, which enables the networks to pick the salient information from the noisy data [44, 41]. Attention can be broadly categorized into two categories viz. implicit attention and explicit attention. During the training, CNNs naturally learn a form of implicit attention where the neurons in CNN respond differently to different parts of input data [24, 23, 47].

Recently, there has been a growing interest in incorporating explicit attention into CNNs for vision-related tasks. Xu et al. [44] and Chen et al. [5] use attention mechanism to generate captions from the images. Wang et al. [37] propose a residual attention network by stacking multiple attention modules to generate attention-aware features. Several other recent works incorporate explicit attention mechanisms to improve the computational efficiency and feature distribution in feature space and improve the efficiency of CNNs. Wang et al. [39] proposed non-local operation, which is a generalized form of self-attention [36], to boost the performance in video recognition tasks. Chen et al. [7] introduced

a double attention block that captures the long-range dependencies by gathering and distributing features in the entire feature space. Park et al. [25] proposed the ‘‘Bottleneck Attention Module’’ (BAM), which employed a multi-layer perceptron (MLP) for channel-wise feature aggregation and dilated convolution for efficiently extracting the spatial information. Woo et al. [42] introduced the ‘‘convolution block attention module’’ (CBAM), which exploits both spatial and channel-wise feature correlation using attention mechanism to improve the representational power of CNNs. SE-Net [15] employed MLP, which re-calibrates the feature maps through squeeze and excitation operations.

To show the efficacy of the aforementioned attention mechanism for compact CNNs, we calculate the computation (FLOPs) and parameter (Params) overhead of deploying these attention mechanisms in CNNs (Table 1). In Table 1, t is the number of attention maps in A^2 - Net and r is the reduction ratio (hyper-parameter) for MLP in BAM, CBAM, and SE-Net. As shown in Table 1, the existing attention mechanisms incur high computational overhead (due to costlier 1×1 convolution used for generating attention maps) and/or parameter overhead (due to the parameter-heavy MLP). On the contrary, ULSAM uses only one 1×1 filter and exploits the linear relationship between feature maps and avoids the use of MLP.

3. Proposed Method

The expressiveness of the self-attention layer with a sufficient number of attention heads and relative positional encoding is higher than that of the convolution layer [10]. However, the large number of attention heads can lead to high compute and parameter overheads, especially in the initial layers of CNNs, where the dimensions of feature maps are high. For example, to replace a convolution layer with 7×7 filters (in the initial layer) with a self-attention layer, at least 49 attention heads need to be deployed [10].

3.1. Design Optimization in ULSAM

In ULSAM, we use only one attention map for each feature subspace. Further, unlike [7] and [39], we use depthwise convolution in the initial step and only one filter in

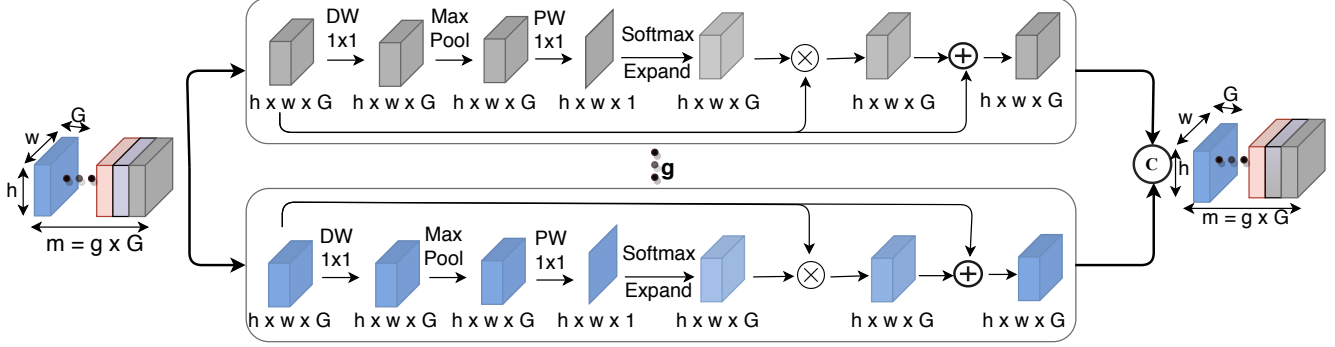


Figure 2. ULSAM divides the input feature maps into g mutually exclusive groups where each group contains G feature maps.

pointwise convolution in the later step of generating the attention maps. This reduces the computations substantially and makes ULSAM suitable for compact CNNs.

Multi-scale feature representation: Multi-scale feature learning helps in understanding the context of the image, especially in a multi-object environment, and improve the representational power of networks [11, 4, 38]. Moreover, multi-scale feature learning enables the network to encode the positional information in an efficient manner, which is desirable for position-dependent vision tasks such as semantic segmentation [16]. Compared to employing the filters of different receptive size (for eg., InceptionNet variants [33, 35, 34]), dividing the feature maps into stages (feature map subspace) and applying different convolution for each stage is an efficient way of generating the multi-scale features which improve the effective receptive size of the networks [11]. Moreover, the predictive performance of network increases with the increasing number of stages in feature map, and hence, compared to increasing depth, width, cardinality, stages in feature maps is a more effective way to boost the representational power of networks [11]. Therefore we divide the feature maps into different subspace and infer different attention maps for each subspace in ULSAM, which enables the multi-scale feature representation.

Multi-frequency feature representation: The natural images composed of low frequency and high-frequency components where the former entails slowly varying features, and the latter represents the fine details in image [6]. Imparting unequal importance to high and low-frequency features is an efficient way of representing features in feature maps [6, 8]. Following this, learning different importance through different weights in different attention maps for each feature subspace is an efficient way of learning multi-frequency features. This way of learning multi-frequency features is beneficial when there are high intra-class variations present in image samples. Hence, multi-frequency features leaning is more desirable for fine-grained image classification where discriminative regions have fine details, i.e., high-frequency features.

3.2. ULSAM

Let $F \in R^{m \times h \times w}$ be the feature maps from an intermediate convolution layer, where m is the number of input channels, h , and w is the spatial dimensions of the feature maps. Our objective is to learn to capture the cross-channel inter-dependencies in the feature maps efficiently. As shown in Figure 2, ULSAM divides the input feature maps (F) into g mutually exclusive groups $[F_1, F_2, \dots, F_{\bar{n}}, \dots, F_g]$ where each group have G feature maps. We define $F_{\bar{n}}$ as a group of intermediate feature maps and proceed as follows.

$$A_{\bar{n}} = \text{softmax}(PW^1(\text{maxpool}^{3 \times 3, 1}(DW^{1 \times 1}(F_{\bar{n}})))) \quad (2)$$

$$\hat{F}_{\bar{n}} = (A_{\bar{n}} \otimes F_{\bar{n}}) \oplus F_{\bar{n}} \quad (3)$$

$$\hat{F} = \text{concat}([\hat{F}_1, \hat{F}_2, \dots, \hat{F}_{\bar{n}}, \dots, \hat{F}_g]) \quad (4)$$

In Eq. 2, $\text{maxpool}^{3 \times 3, 1}$ is maxpool with kernel size = 3×3 and padding = 1, $DW^{1 \times 1}$ is depthwise convolution with 1×1 kernel, PW^1 is pointwise convolution with only one filter, and $A_{\bar{n}}$ is an attention map inferred from a group of intermediate feature maps ($F_{\bar{n}}$). Attention map ($A_{\bar{n}}$) in each group (subspace) captures the non-linear dependencies among the feature maps by learning to gather cross channel information. To ensure $\sum_{i,j} A_{\bar{n}}(i, j) = 1$, i.e. a valid attention weighting tensor, we employ a gating mechanism with a softmax activation in Eq. 2. Each group of feature maps gets the refined set of feature maps ($\hat{F}_{\bar{n}}$) after the feature-redistribution in Eq. 3 where \otimes is element-wise multiplication and \oplus is element-wise addition. The final output of ULSAM (\hat{F}) is obtained by concatenating the feature maps from each group (Eq. 4).

Similar to the squeeze operation in SE-Net [15], depthwise convolution followed by max pool operation, which highlights the local informative regions [46], in Eq. 2 gathers the spatial information. However, unlike the excitation stage in SE-Net, we do not use parameter-heavy MLP to captures the channel-wise inter-dependencies; instead, we exploit the linear relationship between different feature map subspace for integrating the cross-channel information. In

effect, ULSAM learns to capture the complex interaction of cross channel information with very few parameters and computations. We analyze ULSAM by considering three prominent cases.

Case 1: $g = 1$: In this case, there is only one group, i.e., the cross channel information for the whole feature volume is captured by a single attention map. Intuitively, a single attention map is not sufficient to capture the complex relationships in the entire feature space and would result in lower predictive performance.

Case 2 : $1 < g < m$: Dividing the feature maps into g groups implies that g attention maps will be generated. Each attention map can capture the cross channel information from the feature maps in its respective groups. We have performed our experiments (Section 4) with various g (such as $g= 1,4,8,16$) and have obtained performance improvement with higher g ($g = 4, 8, 16$) on ImageNet (Table 6).

Case 3: $g = m$: Here, the attention map is generated for each feature map in feature space. Hence, Eq. 2 can be re-written as: $A_{\bar{n}} = softmax(\alpha_2 \otimes (maxpool^{3 \times 3, 1}(\alpha_1 \otimes F_{\bar{n}})))$. Here α_1 and α_2 are parameters for depthwise and pointwise convolution. In each group, there is only one feature map (i.e., $G = 1$), and nothing is to be learned along the channel dimension. Hence, the attention map will not be able to capture the cross channel information, and the process of generating attention maps reduces to a non-linear transformation of the feature map itself.

Clearly, better interaction of cross-channel information can be obtained when $1 < g < m$ and this intuition is confirmed by the results shown in Table 6. To keep the model simple, we do not employ any intelligent policy for dividing the feature maps into groups. Instead, we divide the feature maps into groups such that G remains the same in all the groups. We notice that *dividing the feature maps into groups does not incur any additional parameter or computation overhead* while learning the cross-channel information effectively. In other words, the storage and computational cost depends only on the number of channels (m) and is independent of the number of groups (g) formed.

4. Experiments and Results

Datasets: We perform image classification on ImageNet-1K [29] and fine-grained datasets, viz., Caltech-UCSD Birds-200-2011 [40] (Birds for short) and Stanford Dogs [17] (Dogs for short) datasets (Table 2). Fine-grained classification is quite challenging due to substantial intra-class variation. Similarly, Food-101 has noisy training samples and high variations in local information. We report validation accuracy (Top-1 and Top-5), an average of three runs, for a single crop input image of size 224×224 . The accuracy reported on fine-grained image classification datasets is obtained by training the models from scratch (not on the ImageNet pre-trained model).

Experimental setup: We perform experiments using PyTorch deep learning framework [26] with MobileNet-V1 (MV1 for short) and MobileNet-V2 (MV2 for short) as baseline architectures. To enable fair comparison, we reproduce the results of baseline CNNs while applying the same training configuration as in baseline + ULSAM. We used four P100 GPUs for ImageNet-1K experiments and two P100 GPUs for fine-grained image classification experiments. We train MV1 and MV1+ULSAM with the batch size of 128 and SGD optimizer with 0.9 momentum for 90 epochs in the case of ImageNet-1K and 150 epochs for fine-grained image classification. The initial learning rate is 0.1, and it reduces to $\frac{1}{10}$ th after every 30 epochs. Similarly, we train MV2 and MV2+ULSAM with batch size 98 and SGD optimizer with 0.9 momentum and $4e-5$ weight decay for 400 epochs on ImageNet-1K and 200 epochs for fine-grained image classification. The initial learning rate is set to 0.045 and decays to $0.98 \times$ after every epoch.

Table 2. Datasets used in experiments

Dataset	#Classes	Size (train/test)	Inter-class variations	Intra-class variations
ImageNet-1K [29]	1000	1.28M/50K	high	low
Food-101 [2]	101	75,750/25,250	low	high
Birds [40]	200	5,994/5,794	low	high
Dogs [17]	120	22K	low	high

Where to insert ULSAM in CNNs? Deeper layers have more semantic information and coarser spatial information in feature maps [28]. Moreover, deeper layers are associated with global features and possess strong positional information [16]. Hence, applying self-attention in deeper layers better learns the interaction of global information as compared to applying attention in initial layers. Furthermore, since the spatial size of feature maps is smaller (as compared to the feature map size in initial layers), employing self-attention in deeper layers is computationally cheaper than applying it in the initial layer s[28]. As shown in Table 3, MV1 has a stack of 5 layers (layers 8-12) with 512 input and output feature maps. Similarly, MobileNet-V2 (MV2) has residual bottleneck blocks from layers 2 to 18 and has different stacks of either 2 or 3 layers with the same configuration (Table 5). These blocks, with repeated layers with the same configuration, incurs very high computation overhead due to a higher number of filters. For example, layers 8 to 12 in MV1 cumulatively account for 46% of total FLOPs in MV1. Therefore, we insert ULSAM between the layers and/or it substitutes the layers from the aforementioned blocks to learn the cross-channel interactions efficiently.

4.1. Results on ImageNet-1K

MV1 and MV2 with additional parameters/FLOPs: We insert ULSAM in MV1 after layer 11, 12, and 13 which is represented as 11:1, 12:1, and 13:1 in Table 6. The pa-

Layer no.	(in, out, stride)
1	conv2d (3, 32, 2)
2,3	DWS (32, 64, 1), (64, 128, 2)
4,5	DWS (128, 128, 1), (128, 256, 2)
6,7	DWS (256, 256, 1), (256, 512, 2)
8-12	DWS $5 \times (512, 512, 1)$
13, 14	DWS (512, 1024, 2), (1024, 1024, 1)
AvgPool, FC, softmax	

Table 4. MobileNet-V1 layers 8 to 12 with ULSAM

Layer no.	Layer type
8	DWS (512, 512, 1)
8:1	ULSAM
9	DWS (512, 512, 1)
9:1	ULSAM
10	DWS (512, 512, 1)
11	ULSAM
12	DWS (512, 512, 1)

Layer no./type	(in, out)
1	conv2d (3, 32)
2	residual block (32, 16)
3-4	residual block $2 \times (16, 24)$
5	residual block (24, 32)
6-7	residual block $2 \times (32, 32)$
8	residual block (32, 64)
9-11	residual block $3 \times (64, 64)$
12	residual block (64, 96)
13-14	residual block $2 \times (96, 96)$
15	residual block (96, 160)
16-17	residual block $2 \times (160, 160)$
18	residual block (160, 320)
19	conv2d (320, 1280)
AvgPool	
20	conv2d (1280, num classes)

Table 6. Image classification accuracy (%) of MV1/MV2 (with additional parameters/FLOPs) + ULSAM ($g = 1, 2, 4, 8, 16$) on ImageNet-1K.

Model	Pos	#Params	#FLOPs	$g = 1$		$g = 2$		$g = 4$		$g = 8$		$g = 16$	
				Top-1	Top-5	Top-1	Top-5	Top-1	Top-5	Top-1	Top-5	Top-1	Top-5
1.0 MV1 (vanilla)	-	4.2M	569M	Top-1 = 70.65, Top-5 = 89.76									
1.0 MV1 + ULSAM	11:1	4.2M	569.2M	70.69	89.85	70.84	89.87	70.77	89.91	70.59	89.83	70.89	89.74
1.0 MV1 + ULSAM	12:1	4.2M	569.2M	70.62	89.86	70.88	89.88	70.61	89.79	70.92	89.98	70.73	89.78
1.0 MV1 + ULSAM	13:1	4.2M	569.1M	70.63	89.60	70.85	89.97	70.86	89.85	70.74	89.81	70.82	90.05
MV2 (vanilla)	-	3.4M	300M	Top-1 = 71.25, Top-5 = 90.19									
MV2 + ULSAM	17:1	3.4M	300.01M	71.31	90.28	71.39	90.34	71.64	90.27	71.35	90.36	71.42	90.43

parameter and FLOPs overhead incurs due to the insertion of ULSAM at position 11:1, 12:1, and 13:1 is 1.02K and 0.2M/0.1M respectively. Top-1 accuracy on ImageNet-1K has increased by 0.27% and 0.21% when position of ULSAM ($g=4/8$) is 12:1 and 13:1, respectively. Similarly, the accuracy of MV2 is increased by 0.39% when ULSAM is inserted after layer 17 (Table 5) and incurs only 0.32K and 0.015M additional parameters and FLOPs respectively (Table 6).

Key observations: For every position of ULSAM, the performance of MV1/MV2 is higher when $g \geq 4$. Specifically, there is a significant gain in the performance of MV1/MV2 when g is increased beyond one. This indicates that separate attention maps for the different parts of ofmaps help in better feature representation.

MV1 and MV2 with fewer parameters/FLOPs: As shown in Table 3, MV1 layers 8 to 12 have the same configuration and they account for 46% of total FLOPs. We use ULSAM to optimize this part of the network by inserting ULSAM after 8th and 9th layers and substitute 11th layer, i.e. at position (8:1, 9:1, 11) shown in Table 4. Compared to baseline network, we achieved a substantial reduction 52M and 0.3M in FLOPs and parameters (respectively) with a 0.22% drop in top-1 accuracy on ImageNet-1K (Table 7).

We further perform experiments on scaled version of

Table 7. Image classification accuracy (%) of MV1 (with fewer parameters and FLOPs) + ULSAM on ImageNet-1K.

Models	Pos	#Params	#FLOPs	Top-1	Top-5
1.0 MV1 (vanilla)	-	4.2M	569M	70.65	89.76
1.0 MV1 + ULSAM ($g = 1$)	(8:1, 9:1, 11)	3.9M	517M	69.92	89.25
1.0 MV1 + ULSAM ($g = 2$)	(8:1, 9:1, 11)	3.9M	517M	70.14	89.67
1.0 MV1 + ULSAM ($g = 4$)	(8:1, 9:1, 11)	3.9M	517M	70.43	89.92
1.0 MV1 + ULSAM ($g = 8$)	(8:1, 9:1, 11)	3.9M	517M	70.29	89.96
1.0 MV1 + ULSAM ($g = 16$)	(8:1, 9:1, 11)	3.9M	517M	70.04	89.98
0.75 MV1 (vanilla)	-	2.6M	325M	67.48	88.00
0.75 MV1 + ULSAM ($g = 1$)	(8:1, 9:1, 11)	2.4M	296M	67.98	88.06
0.75 MV1 + ULSAM ($g = 4$)	(8:1, 9:1, 11)	2.4M	296M	67.81	88.43
0.50 MV1 (vanilla)	-	1.3M	149M	63.22	84.63
0.50 MV1 + ULSAM ($g = 1$)	(8:1, 9:1, 11)	1.2M	136M	63.42	84.70
0.50 MV1 + ULSAM ($g = 4$)	(8:1, 9:1, 11)	1.2M	136M	63.25	84.81

Table 8. Image classification accuracy (%) of MV2 (with fewer parameters and FLOPs) + ULSAM on ImageNet-1K.

Models	Pos	#Params	#FLOPs	Top-1	Top-5
MV2 (Vanilla)	-	3.4M	300M	71.25	90.19
MV2 + ULSAM ($g = 4$)	(14, 17)	2.96M	261.88M	71.52	90.25
MV2 + ULSAM ($g = 4$)	(16, 17)	2.77M	269.07M	70.74	89.15
MV2 + ULSAM ($g = 4$)	(13, 14, 16, 17)	2.54M	223.77M	69.72	87.79

MV1 where the number of filters in each layer is scaled down by a factor of α (where $\alpha \in \{0.5, 0.75\}$). The position of ULSAM is same i.e., (8:1, 9:1, 11) as employed in 1.0-MV1+ULSAM. Since performance of MV1 with ULSAM is highest for $g=4$ (Table 7), we perform our experiments with only $g = 1$ and $g = 4$ for scaled MV1. Table 7 shows the

Table 9. Image classification accuracy (%) of MV1 (with fewer parameters/FLOPs) + ULSAM ($g = 1,4,8,16$) on fine-grained datasets.

Models	Pos	#Params	#FLOPs	Food-101		Birds		Dogs	
				Top-1	Top-5	Top-1	Top-5	Top-1	Top-5
MV1 (vanilla)	-	4.2M	569M	81.31	95.24	62.88	86.05	62.20	89.66
MV1 + ULSAM ($g = 1$)	(8:1, 9:1, 11)	3.9M	517M	81.28	95.50	62.46	86.01	62.73	88.80
MV1 + ULSAM ($g = 4$)	(8:1, 9:1, 11)	3.9M	517M	81.30	95.37	63.52	85.80	63.06	89.58
MV1 + ULSAM ($g = 8$)	(8:1, 9:1, 11)	3.9M	517M	81.19	95.41	64.44	86.60	63.30	89.68
MV1 + ULSAM ($g = 16$)	(8:1, 9:1, 11)	3.9M	517M	81.62	95.33	63.47	84.90	62.75	89.35

Table 10. Image classification accuracy (%) of MV2 (with fewer parameters/FLOPs) + ULSAM ($g = 1,4,8,16$) on Food-101 dataset.

Model	Positions	#Params	#FLOPs	$g = 1$		$g = 4$		$g = 8$		$g = 16$	
				Top-1	Top-5	Top-1	Top-5	Top-1	Top-5	Top-1	Top-5
MV2 (vanilla)	-	3.4M	300M	Top-1 = 81.51, Top-5 = 95.24							
MV2 + ULSAM	13	3.28M	277.34M	81.67	95.82	81.71	95.47	81.76	95.51	81.94	95.63
MV2 + ULSAM	16	3.08M	284.54M	82.05	95.56	82.02	95.48	81.74	95.40	81.54	95.14
MV2 + ULSAM	(9,13)	3.23M	267.06M	81.66	95.36	81.72	95.48	81.88	95.69	81.57	95.30
MV2 + ULSAM	(16,17)	2.77M	269.08M	82.62	95.76	82.40	95.70	82.83	95.81	83.02	95.87
MV2 + ULSAM	(14,17)	2.97M	261.88M	81.57	95.44	81.69	95.36	82.13	95.42	81.84	95.40
MV2 + ULSAM	(13,14,16,17)	2.54M	224.16M	82.38	95.76	82.31	95.80	82.59	95.82	82.91	95.77

results. *Interestingly*, scaled MV1+ULSAM (with both $g=1$ and $g=4$) achieved higher Top-1 accuracy on ImageNet-1K with significantly reduced parameters and FLOPs compared to their baseline. More precisely, the top-1 accuracy of 0.75-MV1+ULSAM($g=1$) is improved by 0.5% with 9.1% and 5.8% fewer FLOPs and parameters while that of 0.50-MV1+ULSAM($g=1$) is improved by 0.10% with 8.92% and 7.69% fewer FLOPs and parameters, respectively.

Similarly, when ULSAM substituted with residual block 14 and 17 in MV2 (Table 5) the top-1 accuracy of MV2 is improved by 0.27% while having 431.6K and 38.2M fewer parameters and FLOPs (Table 8). On substituting layers 13, 14, 16, and 17 with ULSAM, we achieved 25.28% and 25.27% reduction in FLOPs and parameter count, respectively, and the top-1 accuracy is reduced to 69.72%. Thus, *ULSAM either retains or improves accuracy while bringing a significant reduction in the number of parameters and FLOPs.*

Key observations:

- Unlike MV1, the performance of scaled-MV1 and MV2 is increased with fewer parameters and FLOPs as compared to their baseline networks. This implies that ULSAM exploits spatial and channel redundancy in a better when the network is more compact. That is, ULSAM captures better inter-class variation through the interaction of cross-channel information when channel redundancy is low.
- With increasing g , there is a diminishing return in the accuracy of MV1+ULSAM (Table 7) because increasing g reduces the value of G in each group and inhibits the cross-channel information exchange. Also, the top-1 accuracy (70.43%) of MV1+ULSAM on ImageNet-1k is lower. However, the top-5 accuracy is higher than

that of the baseline (except with $g = 1$). This implies that the misclassification, which leads to lower top-1 accuracy, is correctly predicted in top-5 predictions by the MV1+ULSAM.

- For both 0.75-MV1+ULSAM and 0.50-MV1+ULSAM, the highest top-1 accuracy is achieved with $g = 1$ instead of the $g = 4$. Since the scaled versions of MV1 already have fewer feature maps per layer, further dividing the feature maps into groups reduces G (as happened with $g = 4$) and hence, reduces the information present in each group and degrades accuracy. The top-5 accuracy is highest at $g = 4$.

4.2. Results on Fine-grained Image Classification Datasets

We perform our experiments on three fine-grained datasets (Table 2) with $g=1, 4, 8$, and 16.

MobileNet-V1 + ULSAM: The Results for MV1+ULSAM on fine-grained datasets are shown in Table 9. The top-1 accuracy of MV1+ULSAM is improved by 0.31% on Food-101 with $g=16$, 1.56% on Birds dataset with $g=8$, and 1.10% with $g=8$ with 9.14% and 7.14% reduction in FLOPs and parameters compared to baseline networks. The highest top-1 accuracy on Birds and Dogs dataset is achieved with $g = 8$ whereas that on Food-101 is achieved with $g = 16$ (Table 7). Thus, at higher value of g , ULSAM captures the intra-class variation more effectively.

MobileNet-V2 + ULSAM: The experimental results on Food-101, Birds and Dogs datasets are shown in Table 10, Table 11, and Table 12 respectively. The performance of MV2 has significantly improved with a substantial reduction in parameter and FLOPs counts. For example, at posi-

Table 11. Image classification accuracy (%) of MV2 (with fewer parameters/FLOPs) + ULSAM ($g = 1,4,8,16$) on Birds dataset.

Model	Positions	#Params	#FLOPs	$g = 1$		$g = 4$		$g = 8$		$g = 16$	
				Top-1	Top-5	Top-1	Top-5	Top-1	Top-5	Top-1	Top-5
MV2 (vanilla)	–	3.4M	300M	Top-1 = 62.94, Top-5 = 84.92							
MV2 + ULSAM	13	3.28M	277.34M	63.01	85.17	63.05	83.48	63.11	84.79	64.32	84.62
MV2 + ULSAM	16	3.08M	284.54M	63.98	86.22	64.44	84.87	65.03	85.63	63.47	84.45
MV2 + ULSAM	(9,13)	3.23M	267.06M	63.43	85.55	63.47	84.41	63.10	84.96	62.21	84.62
MV2 + ULSAM	(16,17)	2.77M	269.08M	64.19	85.46	64.57	84.92	64.61	85.25	65.03	85.64
MV2 + ULSAM	(14,17)	2.97M	261.88M	63.35	85.29	64.70	86.98	65.41	86.01	63.31	84.92
MV2 + ULSAM	(13,14,16,17)	2.54M	224.16M	64.11	86.77	64.15	84.92	63.22	85.21	63.98	85.12

Table 12. Image classification accuracy (%) of MV2 (with fewer parameters/FLOPs) + ULSAM ($g = 1,4,8,16$) on Dogs dataset.

Model	Pos	#Params	#FLOPs	$g = 1$		$g = 4$		$g = 8$		$g = 16$	
				Top-1	Top-5	Top-1	Top-5	Top-1	Top-5	Top-1	Top-5
MV2 (vanilla)	–	3.4M	300M	Top-1 = 61.81, Top-5 = 86.88							
MV2 + ULSAM	13	3.28M	277.34M	61.63	86.58	61.80	86.68	62.05	87.30	60.31	86.63
MV2 + ULSAM	16	3.08M	284.54M	62.60	88.20	62.90	87.30	63.01	88.00	61.70	87.40
MV2 + ULSAM	(9, 13)	3.23M	267.06M	61.73	87.08	61.73	86.86	62.66	87.86	62.08	88.11
MV2 + ULSAM	(16, 17)	2.77M	269.08M	63.28	88.86	64.30	89.58	64.10	88.58	62.48	88.41
MV2 + ULSAM	(14, 17)	2.97M	261.88M	62.86	87.88	62.50	88.03	64.33	89.31	61.67	87.18
MV2 + ULSAM	(13, 14, 16, 17)	2.54M	224.16M	63.20	88.84	63.53	88.63	62.75	88.18	62.50	88.56

tion (13,14,16,17) the top-1 accuracy of MV2 is improved by 1.4% on Food-101 (with $g=16$), 1.21% on Birds dataset (with $g=4$), and 1.72% on Dogs dataset (with $g=4$) while incurring 25.28% and 25.27% reduction in FLOPs and parameter count, respectively. On all positions of ULSAM, the performance is improved compared to baseline model.

Key Observations: Almost all experiments on fine-grain datasets with different positions of ULSAM perform better than vanilla with significantly lower computations and parameters. This substantiates that applying different weights (through different attention maps) for feature maps with different frequency components boost the representational power significantly on fine-grained datasets.

4.3. Attention visualization

We now show the effectiveness of our approach through human-interpretable visual explanation. We apply the Grad-Cam++ tool [3, 31] on MV1 and MV2 using images from the Birds dataset. Grad-Cam++ provides complete heatmaps of the object, and the masked regions in the images are important (considered by the networks) for predicting the class. Figure 3 shows the visualization results with vanilla MV1 and MV2 and their ULSAM integrated versions. Evidently, ULSAM integrated versions of MobileNet focuses the target images better than the baseline networks, which better explain the effectiveness of ULSAM.

5. Conclusion

We proposed an ultra-lightweight attention block (ULSAM), which divides the feature maps into multiple subspaces to capture the inter-dependencies. The lower parameter and computation overhead of ULSAM, compared to the

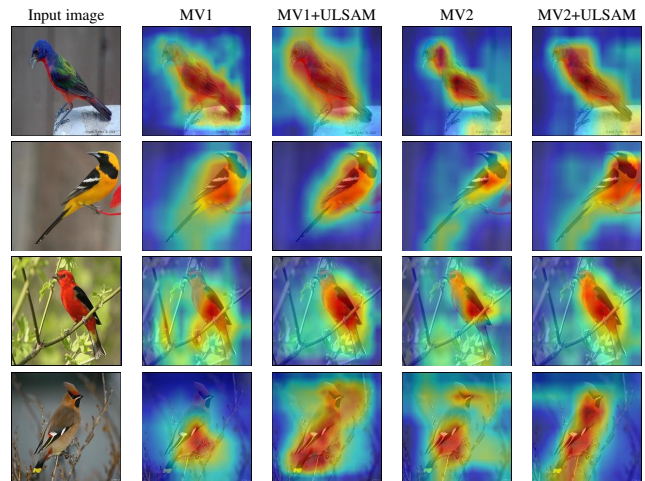


Figure 3. Grad-CAM++ visualization results. Here the input images are Painted bunting, Hooded Oriole, Scarlet Tanager, and Bohemian Waxwing (in order).

state-of-the-art attention mechanism, make it desirable for compact CNNs. Our future work will focus on incorporating spatial attention and capturing complex global relations in the entire feature space of CNNs.

Acknowledgments

We thank anonymous reviewers for their invaluable feedback and insightful reviews. We thank TRI-AD for the travel grant. This project was supported in part by Semiconductor research corporation (SRC) and by Science and Engineering Research Board (SERB), India, award number ECR/2017/000622.

References

- [1] I. Bello, B. Zoph, A. Vaswani, J. Shlens, and Q. V. Le. Attention augmented convolutional networks. *ICCV*, 2019.
- [2] L. Bossard, M. Guillaumin, and L. Van Gool. Food-101 – mining discriminative components with random forests. In *Computer Vision – ECCV 2014*, pages 446–461, 2014.
- [3] A. Chattopadhyay, A. Sarkar, P. Howlader, and V. N. Balasubramanian. Grad-cam++: Generalized gradient-based visual explanations for deep convolutional networks. In *2018 IEEE Winter Conference on Applications of Computer Vision (WACV)*, pages 839–847, March 2018.
- [4] C.-F. R. Chen, Q. Fan, N. Mallinar, T. Sercu, and R. Feris. Big-little net: An efficient multi-scale feature representation for visual and speech recognition. In *International Conference on Learning Representations*, 2019.
- [5] L. Chen, H. Zhang, J. Xiao, L. Nie, J. Shao, W. Liu, and T.-S. Chua. Sca-cnn: Spatial and channel-wise attention in convolutional networks for image captioning. In *The IEEE Conference on Computer Vision and Pattern Recognition (CVPR)*, pages 5659–5667, July 2017.
- [6] Y. Chen, H. Fan, B. Xu, Z. Yan, Y. Kalantidis, M. Rohrbach, S. Yan, and J. Feng. Drop an octave: Reducing spatial redundancy in convolutional neural networks with octave convolution. *Proceedings of the IEEE International Conference on Computer Vision*, 2019.
- [7] Y. Chen, Y. Kalantidis, J. Li, S. Yan, and J. Feng. A²-nets: Double attention networks. In *Advances in Neural Information Processing Systems 31*, pages 352–361. 2018.
- [8] B. Cheng, R. Xiao, J. Wang, T. Huang, and L. Zhang. High frequency residual learning for multi-scale image classification. *BMVC*, 2019.
- [9] F. Chollet. Xception: Deep learning with depthwise separable convolutions. In *The IEEE Conference on Computer Vision and Pattern Recognition (CVPR)*, July 2017.
- [10] J.-B. Cordonnier, A. Loukas, and M. Jaggi. On the relationship between self-attention and convolutional layers. In *International Conference on Learning Representations*, 2020.
- [11] S.-H. Gao, M.-M. Cheng, K. Zhao, X.-Y. Zhang, M.-H. Yang, and P. Torr. Res2net: A new multi-scale backbone architecture. *IEEE TPAMI*, 2019.
- [12] K. He, X. Zhang, S. Ren, and J. Sun. Deep residual learning for image recognition. In *The IEEE Conference on Computer Vision and Pattern Recognition (CVPR)*, pages 770–778, June 2016.
- [13] K. He, X. Zhang, S. Ren, and J. Sun. Identity mappings in deep residual networks. In B. Leibe, J. Matas, N. Sebe, and M. Welling, editors, *Computer Vision – ECCV 2016*, pages 630–645. Cham, 2016. Springer International Publishing.
- [14] A. G. Howard et al. Mobilenets: Efficient convolutional neural networks for mobile vision applications. *CoRR*, abs/1704.04861, 2017.
- [15] J. Hu, L. Shen, and G. Sun. Squeeze-and-excitation networks. In *The IEEE Conference on Computer Vision and Pattern Recognition (CVPR)*, pages 7132–7141, June 2018.
- [16] M. A. Islam, S. Jia, and N. D. B. Bruce. How much position information do convolutional neural networks encode? In *International Conference on Learning Representations*, 2020.
- [17] A. Khosla, N. Jayadevaprakash, B. Yao, and L. Fei-Fei. Novel dataset for fine-grained image categorization. In *First Workshop on Fine-Grained Visual Categorization, IEEE Conference on Computer Vision and Pattern Recognition*, Colorado Springs, CO, June 2011.
- [18] A. Krizhevsky, I. Sutskever, and G. E. Hinton. Imagenet classification with deep convolutional neural networks. In *Advances in Neural Information Processing Systems 25*, pages 1097–1105. 2012.
- [19] Y. Lecun, L. Bottou, Y. Bengio, and P. Haffner. Gradient-based learning applied to document recognition. *Proceedings of the IEEE*, 86(11):2278–2324, Nov 1998.
- [20] M. Lin, Q. Chen, and S. Yan. Network in network. *CoRR*, 2013.
- [21] N. Ma, X. Zhang, H.-T. Zheng, and J. Sun. Shufflenet v2: Practical guidelines for efficient cnn architecture design. In *The European Conference on Computer Vision (ECCV)*, September 2018.
- [22] H. Mhaskar, Q. Liao, and T. A. Poggio. Learning real and boolean functions: When is deep better than shallow. *CoRR*, abs/1603.00988, 2016.
- [23] C. Olah, A. Mordvintsev, and L. Schubert. Feature visualization. *Distill*, 2017. <https://distill.pub/2017/feature-visualization>.
- [24] C. Olah, A. Satyanarayan, I. Johnson, S. Carter, L. Schubert, K. Ye, and A. Mordvintsev. The building blocks of interpretability. *Distill*, 2018. <https://distill.pub/2018/building-blocks>.
- [25] J. Park, S. Woo, J. Lee, and I. S. Kweon. BAM: bottleneck attention module. In *British Machine Vision Conference 2018, BMVC 2018*, page 147, 2018.
- [26] A. Paszke, S. Gross, S. Chintala, G. Chanan, E. Yang, Z. DeVito, Z. Lin, A. Desmaison, L. Antiga, and A. Lerer. Automatic differentiation in pytorch. 2017.
- [27] T. A. Poggio, H. Mhaskar, L. Rosasco, B. Miranda, and Q. Liao. Why and when can deep-but not shallow-networks avoid the curse of dimensionality: A review. *International Journal of Automation and Computing*, 14:503–519, 2017.
- [28] P. Ramachandran, N. Parmar, A. Vaswani, I. Bello, A. Levskaya, and J. Shlens. Stand-alone self-attention in vision models. *NeurIPS*, 2019.
- [29] O. Russakovsky, J. Deng, H. Su, J. Krause, S. Satheesh, S. Ma, Z. Huang, A. Karpathy, A. Khosla, M. Bernstein, A. C. Berg, and L. Fei-Fei. Imagenet large scale visual recognition challenge. *International Journal of Computer Vision (IJCV)*, 115(3):211–252, 2015.
- [30] M. Sandler et al. Mobilenetv2: Inverted residuals and linear bottlenecks. In *2018 IEEE/CVF Conference on Computer Vision and Pattern Recognition*, pages 4510–4520, June 2018.
- [31] R. R. Selvaraju, M. Cogswell, A. Das, R. Vedantam, D. Parikh, and D. Batra. Grad-cam: Visual explanations from deep networks via gradient-based localization. In *The IEEE International Conference on Computer Vision (ICCV)*, Oct 2017.
- [32] K. Simonyan and A. Zisserman. Very deep convolutional networks for large-scale image recognition. *CoRR*, abs/1409.1556, 2014.

- [33] C. Szegedy et al. Going deeper with convolutions. In *CVPR*, June 2015.
- [34] C. Szegedy et al. Inception-v4, inception-resnet and the impact of residual connections on learning. In *AAAI*, 2017.
- [35] C. Szegedy, V. Vanhoucke, S. Ioffe, J. Shlens, and Z. Wojna. Rethinking the inception architecture for computer vision. In *CVPR*, June 2016.
- [36] A. Vaswani, N. Shazeer, N. Parmar, J. Uszkoreit, L. Jones, A. N. Gomez, L. u. Kaiser, and I. Polosukhin. Attention is all you need. In *Advances in Neural Information Processing Systems 30*, pages 5998–6008. 2017.
- [37] F. Wang, M. Jiang, C. Qian, S. Yang, C. Li, H. Zhang, X. Wang, and X. Tang. Residual attention network for image classification. In *The IEEE Conference on Computer Vision and Pattern Recognition (CVPR)*, pages 3156–3164, July 2017.
- [38] H. Wang, A. Kembhavi, A. Farhadi, A. L. Yuille, and M. Rastegari. Elastic: Improving cnns with dynamic scaling policies. In *The IEEE Conference on Computer Vision and Pattern Recognition (CVPR)*, June 2019.
- [39] X. Wang, R. Girshick, A. Gupta, and K. He. Non-local neural networks. In *The IEEE Conference on Computer Vision and Pattern Recognition (CVPR)*, pages 7794–7803, June 2018.
- [40] P. Welinder, S. Branson, T. Mita, C. Wah, F. Schroff, S. Belongie, and P. Perona. Caltech-UCSD Birds 200. Technical Report CNS-TR-2010-001, California Institute of Technology, 2010.
- [41] L. Weng. Attention? attention! <https://lilianweng.github.io/lil-log/2018/06/24/attention-attention.html>, 2018.
- [42] S. Woo, J. Park, J.-Y. Lee, and I. So Kweon. Cbam: Convolutional block attention module. In *The European Conference on Computer Vision (ECCV)*, September 2018.
- [43] S. Xie, R. Girshick, P. Dollar, Z. Tu, and K. He. Aggregated residual transformations for deep neural networks. In *The IEEE Conference on Computer Vision and Pattern Recognition (CVPR)*, pages 1492–1500, July 2017.
- [44] K. Xu, J. Ba, R. Kiros, K. Cho, A. Courville, R. Salakhudinov, R. Zemel, and Y. Bengio. Show, attend and tell: Neural image caption generation with visual attention. In F. Bach and D. Blei, editors, *Proceedings of the 32nd International Conference on Machine Learning*, volume 37 of *Proceedings of Machine Learning Research*, pages 2048–2057, Lille, France, 07–09 Jul 2015. PMLR.
- [45] F. Yu and V. Koltun. Multi-scale context aggregation by dilated convolutions. In *International Conference on Learning Representations*, 2016.
- [46] S. Zagoruyko and N. Komodakis. Paying more attention to attention: Improving the performance of convolutional neural networks via attention transfer. In *5th International Conference on Learning Representations, ICLR 2017, Toulon, France, April 24-26, 2017, Conference Track Proceedings*, 2017.
- [47] M. D. Zeiler and R. Fergus. Visualizing and understanding convolutional networks. In D. Fleet, T. Pajdla, B. Schiele, and T. Tuytelaars, editors, *Computer Vision – ECCV 2014*, pages 818–833, Cham, 2014. Springer International Publishing.
- [48] X. Zhang, X. Zhou, M. Lin, and J. Sun. Shufflenet: An extremely efficient convolutional neural network for mobile devices. In *The IEEE Conference on Computer Vision and Pattern Recognition (CVPR)*, pages 6848–6856, June 2018.